

Supplementary information

Enhancing photocatalytic hydrogen peroxide production by doping trace amount of azo linked C₃N₅ in g-C₃N₄ matrix

Ramesh Mandal, Varshit Malla, Arpita Guchhait and Santanu Bhattacharyya*

Section 1. Band gap calculation from UV-Vis diffuse reflectance spectra

First, the resulting UV-vis diffuse reflectance spectra were converted to absorption spectra using the Kubelka-Munk equation.¹

$$F(R) = \frac{(1 - R)^2}{2R} \times 100\% \quad (1)$$

Where R is the reflectance of the corresponding samples. Now, band gap was calculated by using the Tauc equation (2).¹

$$F(R)hv = A(hv - E_g)^{\frac{n}{2}} \quad (2)$$

Where h, v, A and E_g denote Planck constant, light frequency, proportionality constant and band gap respectively. Where, 'n' depends on the nature of transition in semiconductor. Where the values of 'n' are 1, 3, 4, and 6 which are attributed to the allowed direct, forbidden direct, allowed indirect, and forbidden indirect transitions, respectively.^{2,3} From the plot of $(F(R)hv)^{\frac{2}{n}}$ vs. hv, the band gaps of the samples were determined, which are corresponding to the intercept of the extrapolated linear portion of the plot near the band edge with the x-axis. The g-C₃N₄ samples were found to be semiconductors with allowed indirect transition.

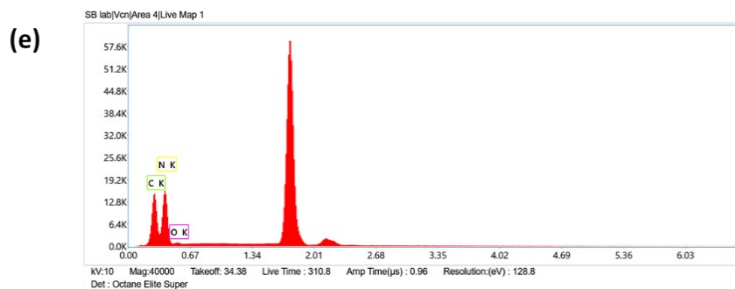
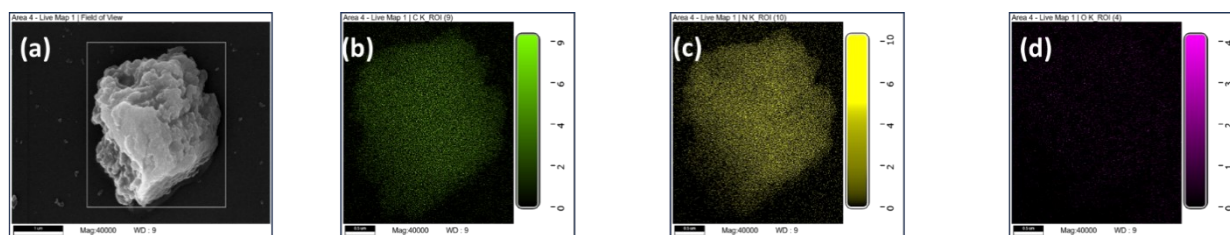


Fig. S1 EDX elemental mapping (a-d) of carbon (C), nitrogen (N), oxygen (O) of C_3N_4 respectively and (e) elemental maps.

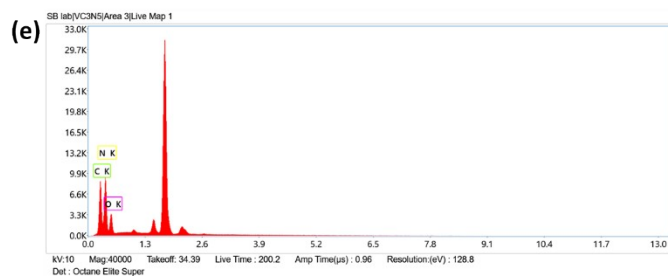
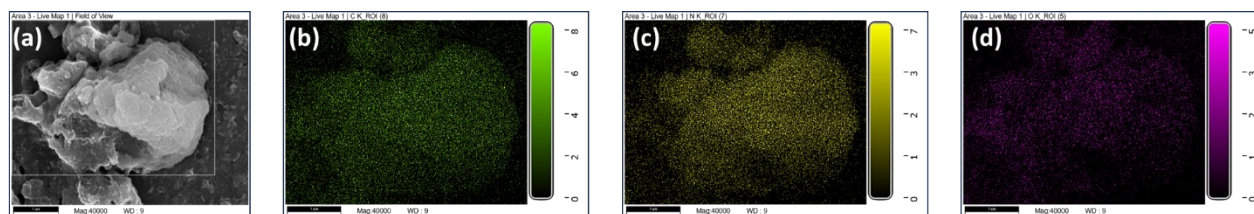


Fig. S2 EDX elemental mapping (a-d) of carbon (C), nitrogen (N), oxygen (O) of C_3N_5 respectively and (e) elemental maps.

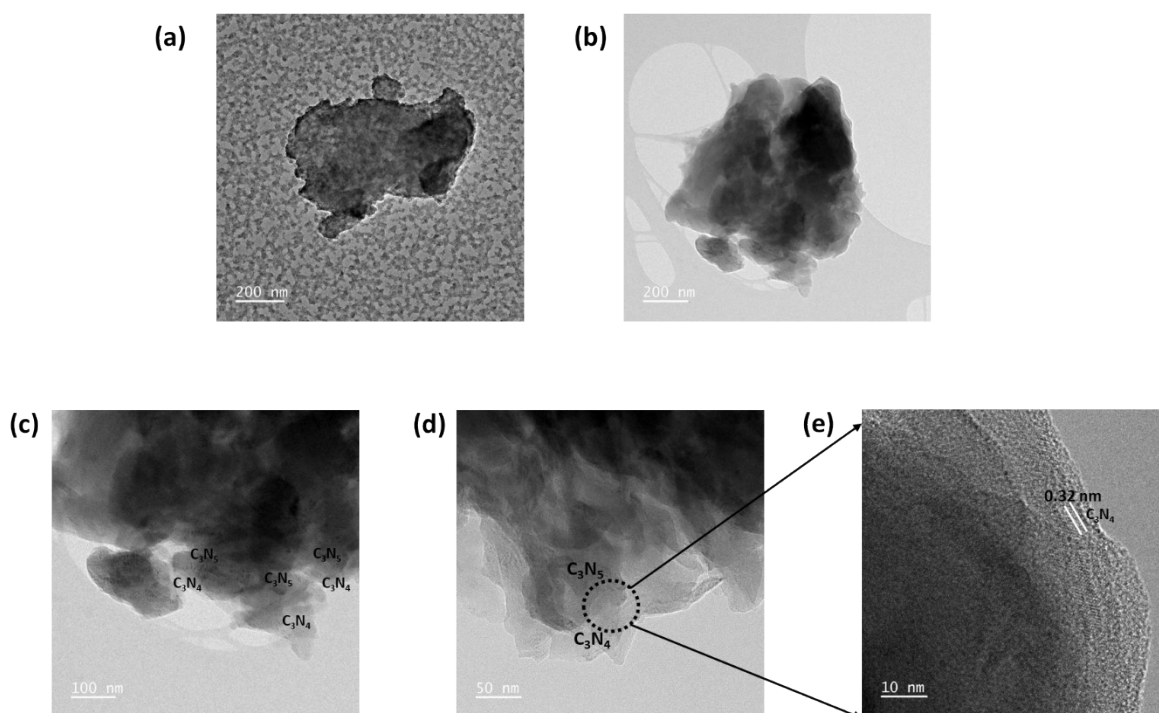


Fig. S3 HRTEM images of (a) C_3N_4 and (b, c, d, e) C_3N_4/C_3N_5 (5%) respectively.

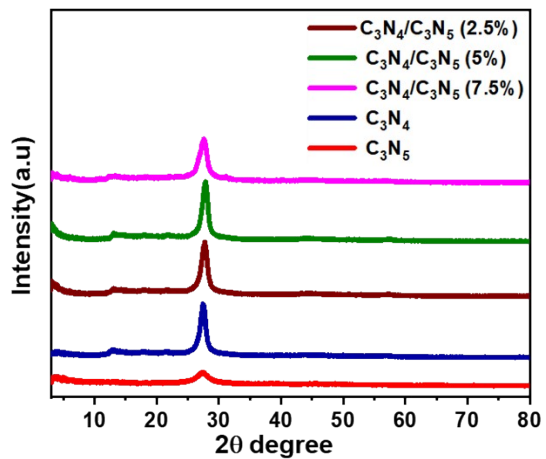


Fig. S4 XRD patterns of C_3N_4 , C_3N_5 , C_3N_4/C_3N_5 (2.5%), C_3N_4/C_3N_5 (5%) and C_3N_4/C_3N_5 (7.5%) samples.

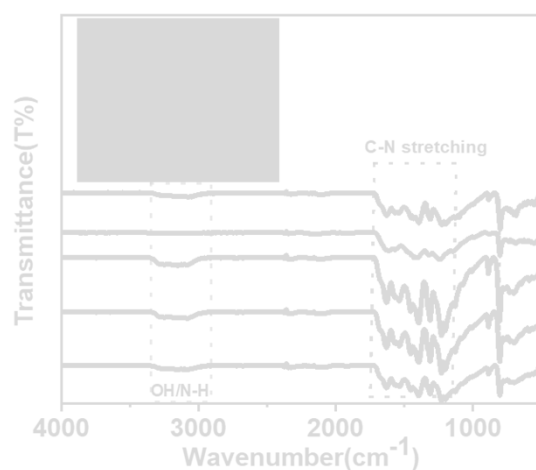


Fig. S5 FTIR spectrum of C_3N_4 , C_3N_5 , C_3N_4/C_3N_5 (2.5%), C_3N_4/C_3N_5 (5%) and C_3N_4/C_3N_5 (7.5%) samples.

Table S1. Quantitative details for the BET surface areas and pore volumes.

Samples	Surface area ($m^2 g^{-1}$)	pore volume ($cm^3 g^{-1}$)
C_3N_4	9.2 ($m^2 g^{-1}$)	0.058 ($cm^3 g^{-1}$)
C_3N_5	12 ($m^2 g^{-1}$)	0.059 ($cm^3 g^{-1}$)
C_3N_4/C_3N_5 (5%)	23 ($m^2 g^{-1}$)	0.1518 ($cm^3 g^{-1}$)

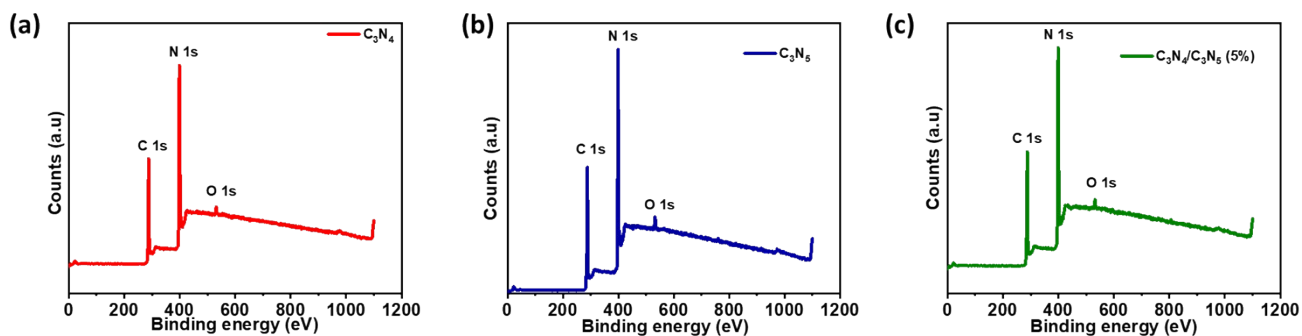


Fig. S6 (a, b, c) XPS survey spectra of C_3N_4 , C_3N_5 , and C_3N_4/C_3N_5 (5%) samples respectively.

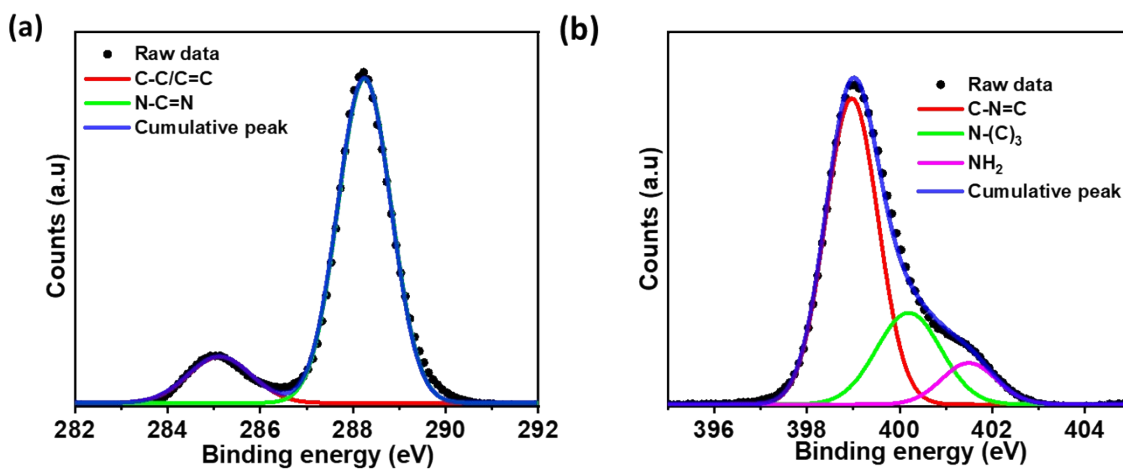


Fig. S7. Deconvoluted high resolution C 1s spectra (a), N 1s spectra (b), of C_3N_5 respectively.

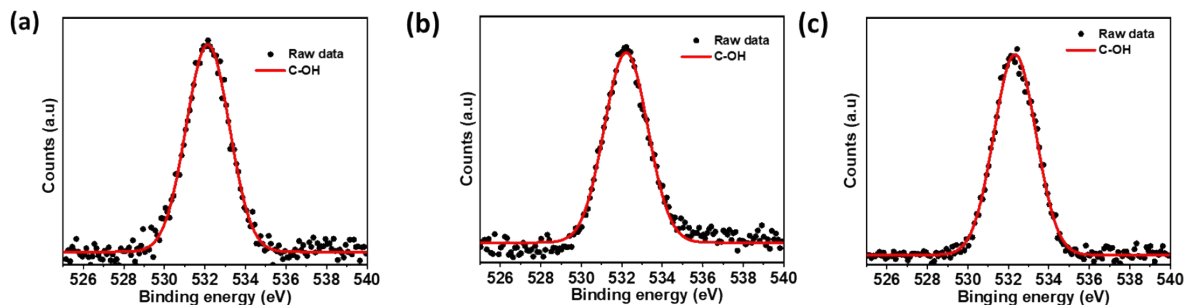


Fig. S8 Deconvoluted high resolution O 1s spectra (a, b, c) of C_3N_4 , C_3N_4/C_3N_5 (5%) and C_3N_5 respectively.

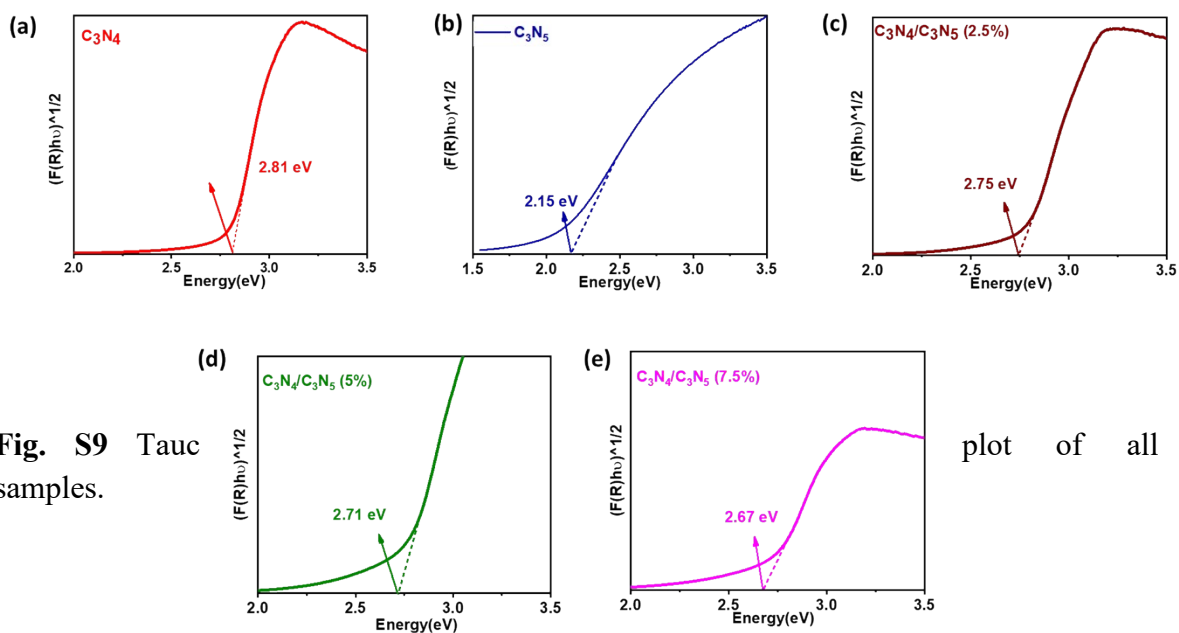


Fig. S9 Tauc samples.

plot of all the

Table S2. Band gap values of the samples.

Samples	Band gap (eV)
C_3N_4	2.81
C_3N_5	2.15
C_3N_4/C_3N_5 (2.5%)	2.75
C_3N_4/C_3N_5 (5%)	2.71
C_3N_4/C_3N_5 (7.5%)	2.67

Table S3. The corresponding exponential decay-fitted parameters of fluorescence lifetime for C_3N_4 , C_3N_5 , C_3N_4/C_3N_5 (2.5%), C_3N_4/C_3N_5 (5%) and C_3N_4/C_3N_5 (7.5%) samples respectively.

Sample name	α_1	α_2	τ_1 (ns)	τ_2 (ns)	τ_{avg} (ns)
C_3N_4	0.67	0.33	1.91	6.67	3.75
C_3N_5	0.52	0.48	0.53	0.56	0.54
$C_3N_4@C_3N_5$ (2.5%)	0.69	0.31	1.27	5.67	2.63
$C_3N_4@C_3N_5$ (5%)	0.67	0.33	1.21	5.25	2.54
$C_3N_4@C_3N_5$ (7.5%)	0.70	0.30	1.01	4.74	2.13

A bi-exponential function was used to analyze and the average PL lifetime (τ_{avg}) was deduced by using the following equation.

$$\tau_{avg} = \alpha_1\tau_1 + \alpha_2\tau_2 \quad (3)$$

Table S4. Decay kinetics parameters probed at 572 nm of pristine C_3N_4 and C_3N_4/C_3N_5 (5%) samples.

Sample name	α_1	τ_1 (ps)	α_2	τ_2 (ps)
Pristine C_3N_4	0.398	3.156	0.588	1434
C_3N_4/C_3N_5 (5%)	0.355	1.726	0.574	1426

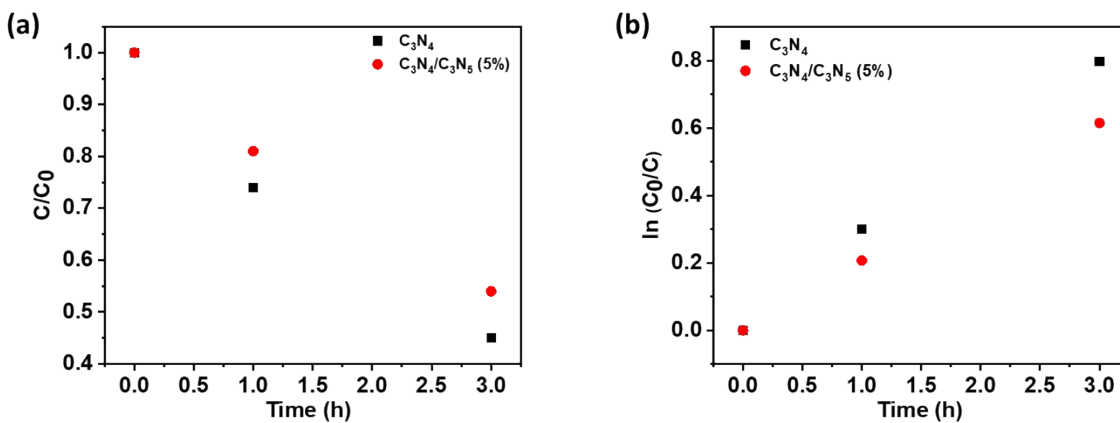
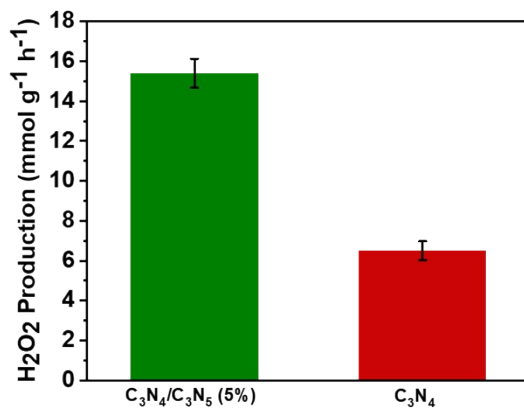


Fig. S10 (a) The H_2O_2 over the catalysts. (b) the decomposition of



photocatalytic decomposition of C_3N_4 & C_3N_4/C_3N_5 (5%) fitting parameters of the H_2O_2 .

Fig. S11 H_2O_2 production over pristine C_3N_4 and $\text{C}_3\text{N}_4/\text{C}_3\text{N}_5$ (5%) samples after 6 h.

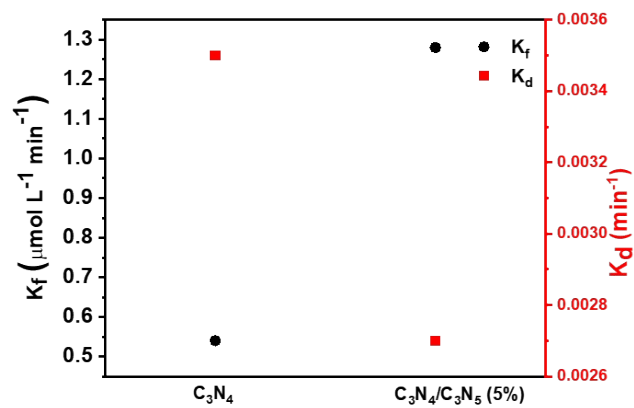


Fig. S12 Formation (K_f) and decomposition rate constants (K_d) for H_2O_2 production after 6 h.

Section 2. Calculation of AQY:

Table S5:

Wavelength (nm)	AQY(%)
350	18.10
380	27.87
420	22.35
480	10.48
530	6.35
550	3.0

The following equation (4) was used to calculate AQY.

$$\text{AQY} = \frac{N_e}{N_p} \times 100\% = \frac{2 \times M \times N_A \times h \times c}{S \times P \times t \times \lambda} \times 100\% \quad (4)$$

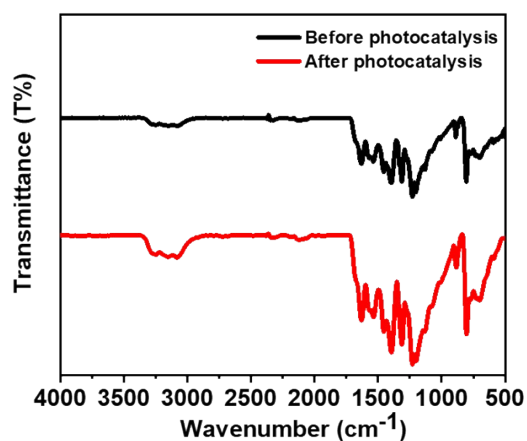


Fig. S13 FTIR spectra of the used photocatalyst before and after photocatalysis experiment.

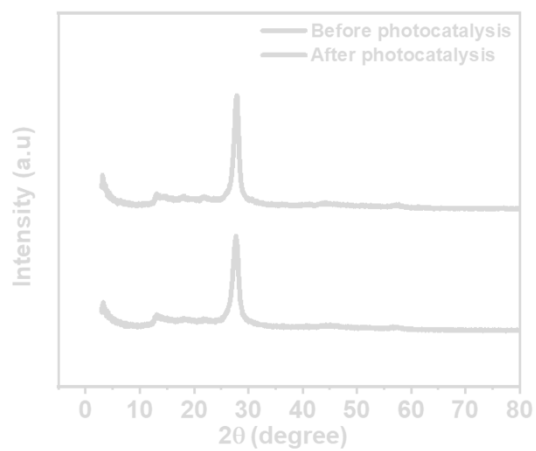


Fig. S14 Powder XRD spectra of the used photocatalyst before and after photocatalysis experiment.

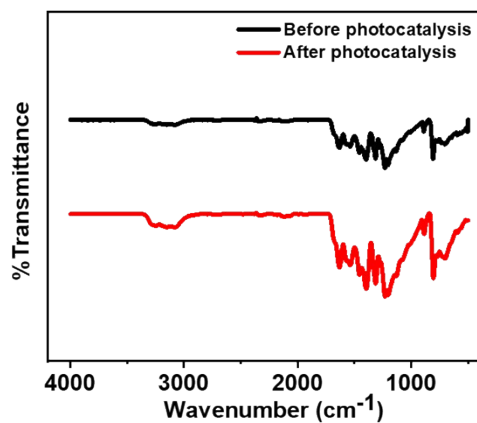


Fig. S15 FTIR spectra of the used photocatalyst before and after cyclic stability experiment for 30 h.

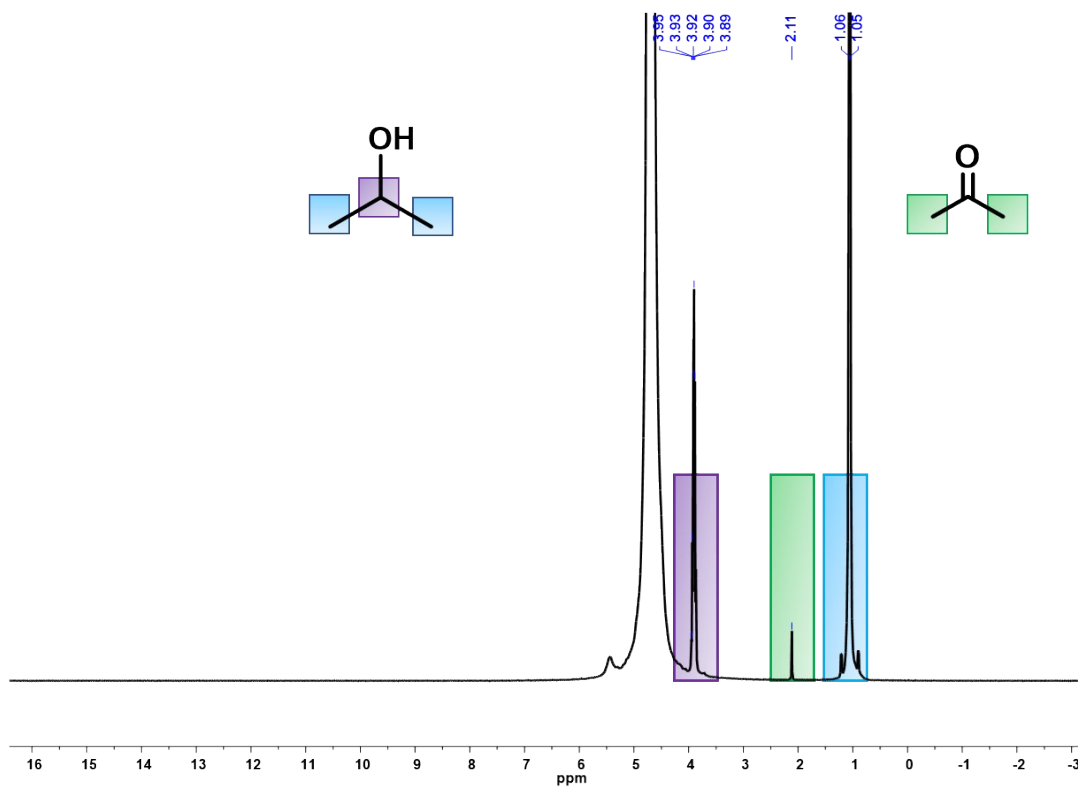


Fig. S16 ^1H NMR spectra of the reaction mixture after photocatalysis process in D_2O solvent.

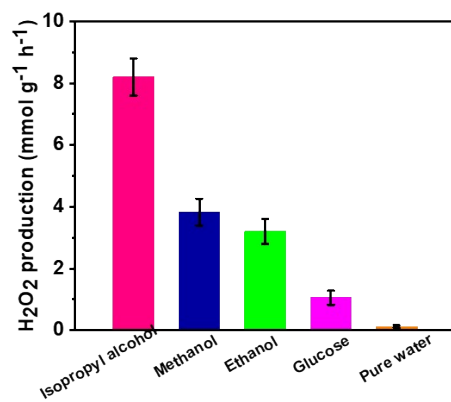


Fig. S17 H_2O_2 production under different hole scavengers and pure water.

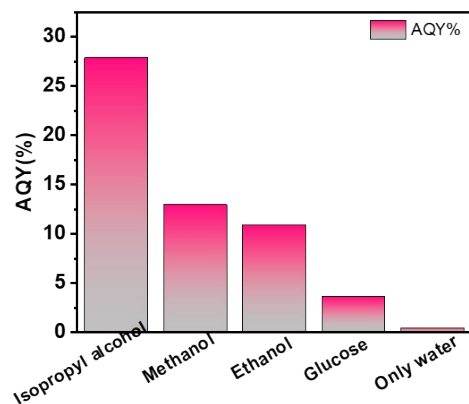


Fig. S18 The AQY values of C_3N_4/C_3N_5 (5%) composite over the different sacrificial donors including pure water at 380 nm.

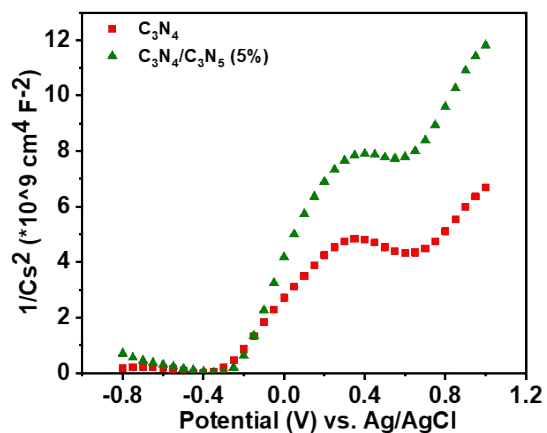


Fig. S19 Mott-Schottky measurements of pristine C_3N_4 and C_3N_4/C_3N_5 (5%) samples.

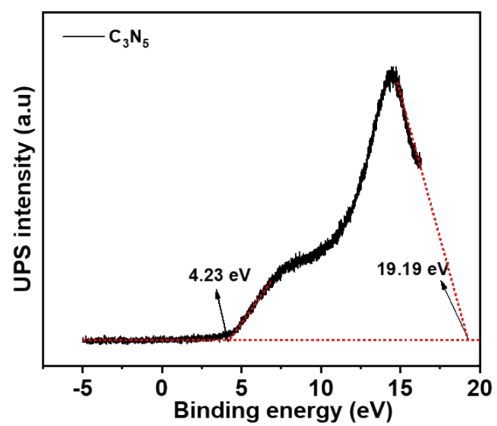


Fig. S20 UPS spectrum of C₃N₅.

References

- 1 D. Zhao, Y. Wang, C.-L. Dong, Y.-C. Huang, J. Chen, F. Xue, S. Shen and L. Guo, *Nat. Energy*, 2021, **6**, 388–397.
- 2 Q. Liang, Z. Li, Z. Huang, F. Kang and Q. Yang, *Adv. Funct. Mater.*, 2015, **25**, 6885–6892.
- 3 R. Mandal and S. Bhattacharyya, *J. Phys. Chem. C*, 2024, **128**, 17342–17352.